

Negative feedback that improves information transmission in yeast signalling

Richard C. Yu¹, C. Gustavo Pesce¹, Alejandro Colman-Lerner^{1†}, Larry Lok^{1†}, David Pincus^{1†}, Eduard Serra^{1†}, Mark Holl^{2†}, Kirsten Benjamin^{1†}, Andrew Gordon^{1†} & Roger Brent¹

Haploid *Saccharomyces cerevisiae* yeast cells use a prototypic cell signalling system to transmit information about the extracellular concentration of mating pheromone secreted by potential mating partners. The ability of cells to respond distinguishably to different pheromone concentrations depends on how much information about pheromone concentration the system can transmit. Here we show that the mitogen-activated protein kinase Fus3 mediates fast-acting negative feedback that adjusts the dose response of the downstream system response to match the dose response of receptor-ligand binding. This 'dose-response alignment', defined by a linear relationship between receptor occupancy and downstream response, can improve the fidelity of information transmission by making downstream responses corresponding to different receptor occupancies more distinguishable and reducing amplification of stochastic noise during signal transmission. We also show that one target of the feedback is a previously uncharacterized signal-promoting function of the regulator of G-protein signalling protein Sst2. Our work suggests that negative feedback is a general mechanism used in signalling systems to align dose responses and thereby increase the fidelity of information transmission.

Cells use signalling systems to sense and transmit information about extracellular conditions. Haploid *Saccharomyces cerevisiae* yeast cells use a prototypic, G-protein-coupled-receptor/mitogen-activated protein kinase (MAPK) cascade signalling system, the pheromone response system¹, to sense and transmit information about the concentration of mating pheromone secreted by cells of the opposite mating type (Fig. 1). The more information about pheromone concentration the system can transmit, the better a cell can distinguish between different pheromone concentrations, an essential ability for proper partner choice and mating. For example, a yeast cell ringed by potential mating partners strongly prefers to mate with partners producing the most pheromone². Partner choice involves two processes that require sensing of pheromone concentration. First, a cell grows up the pheromone concentration gradient³, a process that probably depends on measurement of precise differences in pheromone concentration at different points on the cell surface. Second, after contacting its partner and forming a prezygote, a cell preferentially completes fusion and forms a diploid with a partner that produces high amounts of pheromone⁴. These experiments indicate that it is important for cells to distinguish among different pheromone concentrations at multiple steps during the mating process.

Previous work suggested that optimal transmission of information about pheromone concentration depends on both distinguishable receptor occupancies and distinguishable downstream system responses. Differences in receptor occupancy are clearly important for mating partner choice and discrimination; for example, in the presence of pheromone at a concentration that saturates the receptor, cells lose the ability to discriminate between high-concentration

pheromone-secreting partners and low-concentration pheromone-secreting partners². However, distinguishable receptor occupancies are not sufficient for partner discrimination, as hypersensitive cells, in the presence of pheromone at a concentration that does not saturate the receptor but does saturate downstream responses, also lose the ability to discriminate between partners secreting different levels of pheromone². One complementary study of mating projection orientation in spatial gradients of pheromone showed that hypersensitive cells do not orient their mating projections as precisely as wild-type cells, perhaps because in these cells downstream responses were saturated at most points in the gradient³. However, even in pheromone gradient concentrations 100-fold lower, at which downstream responses should not have been saturated, hypersensitive cells still oriented their mating projections less precisely than did wild-type cells in higher concentration gradients³. These observations suggest that hypersensitive cells are inherently less able to respond distinguishably to different pheromone concentrations (that is, transmit less information about pheromone concentration), even when they are responding to pheromone concentrations that saturate neither receptor nor downstream responses.

Distinguishable responses and dose-response alignment

One characteristic of wild-type cells that we⁵ and others⁶ have previously found is that, despite the large number of intermediate signalling events in the system, the dose-response curve of receptor occupancy closely aligns with dose-response curves of downstream system responses. For example, we observe 'dose-response alignment' between receptor occupancy and the accumulated amount

¹Molecular Sciences Institute, 2168 Shattuck Avenue, Berkeley, California 94704, USA. ²Microscale Life Sciences Center, University of Washington, Seattle, Washington 98195, USA. [†]Present addresses: Instituto de Fisiología, Biología Molecular y Neurociencias, CONICET and Departamento de Fisiología, Biología Molecular y Celular, Facultad de Ciencias Exactas y Naturales, Universidad de Buenos Aires, Argentina (A.C.-L.); Synopsys, Mountain View, California 94043, USA (L.L.); Department of Cellular and Molecular Pharmacology, University of California, San Francisco, California 94158, USA (D.P.); Centre de Genètica Mèdica i Molecular, Institut d'Investigació Biomèdica de Bellvitge (IDIBELL), Barcelona 08907, Spain (E.S.); Biodesign Institute, Arizona State University, Tempe, Arizona 85387, USA (M.H.); Amyris Biotechnologies, Emeryville, California 94608, USA (K.B.); Physics Department, Brookhaven National Laboratory, Upton, New York 11973, USA (A.G.).

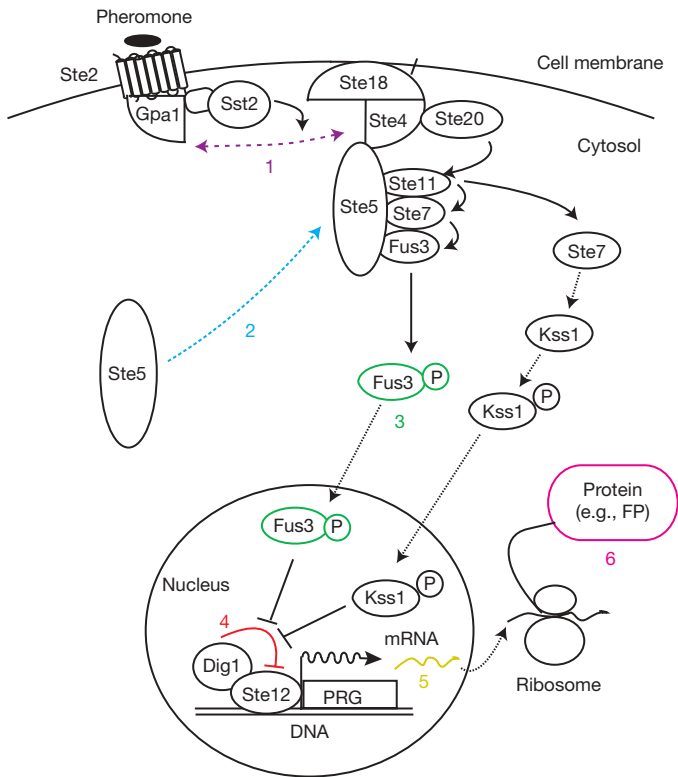


Figure 1 | The pheromone response system. Proteins are indicated by labelled ovals, translocation by dotted arrows, protein activation by arrows, inhibition by T-bar arrows, and protein association by double-headed dashed arrows. Pheromone binding by receptor Ste2 causes dissociation of the heterotrimeric G-protein (1) into $G\alpha$ subunit (Gpa1) and the $G\beta\gamma$ dimer (Ste4–Ste18). GTP-activating protein (GAP) function of the RGS protein Sst2 promotes re-association of Gpa1 with Ste4–Ste18. On dissociation of the G protein, Ste4 helps recruit the MAPK scaffold Ste5 to the membrane (2). Ste5 recruitment activates the MAPK cascade, in which Ste20, Ste11, Ste7 and the MAP kinases Fus3 and Kss1 phosphorylate one another in sequence. Phosphorylated Fus3 (3) translocates to the nucleus and phosphorylates Dig1 and Ste12, eliminating Dig1 repression of Ste12, a transcriptional activator (4). Ste12 activates transcription of pheromone-responsive genes (PRGs) (5, 6).

of pheromone-activated Ste12 (cumulative pathway subsystem output P since system induction, where P is operationally defined by reporter-gene expression corrected for inherent cell-to-cell differences in the ability to express proteins⁵; Fig. 2a). Notably, dose-response alignment is commonly observed in many mammalian cell signalling systems, including the insulin⁷, acetylcholine⁸, thyroid stimulating hormone⁹, angiotensin II¹⁰, and epidermal growth factor^{11,12} response systems. Researchers in the past have often regarded alignment of curves for ligand binding by a candidate receptor and downstream response as evidence that the putative receptor was in fact the molecule that bound ligand and caused the cellular responses^{13–15}. However, to our knowledge, researchers have investigated neither the implications of dose-response alignment for yeast pheromone response nor its general consequences for the function of cell signalling systems.

We realized that dose-response alignment improves information transmission in two ways. First, dose-response alignment describes a linear relationship between receptor occupancy and downstream response; consequently, the entire range of receptor occupancies evenly corresponds to the entire range of possible responses (Fig. 2b). By contrast, even a modest dose-response misalignment, such as a 20-fold shift in the effector concentration for half-maximum response (EC_{50}) of downstream response (Fig. 2c), compresses the downstream responses corresponding to a wide range of receptor occupancies into a narrow range (Fig. 2d). Second, dose-response

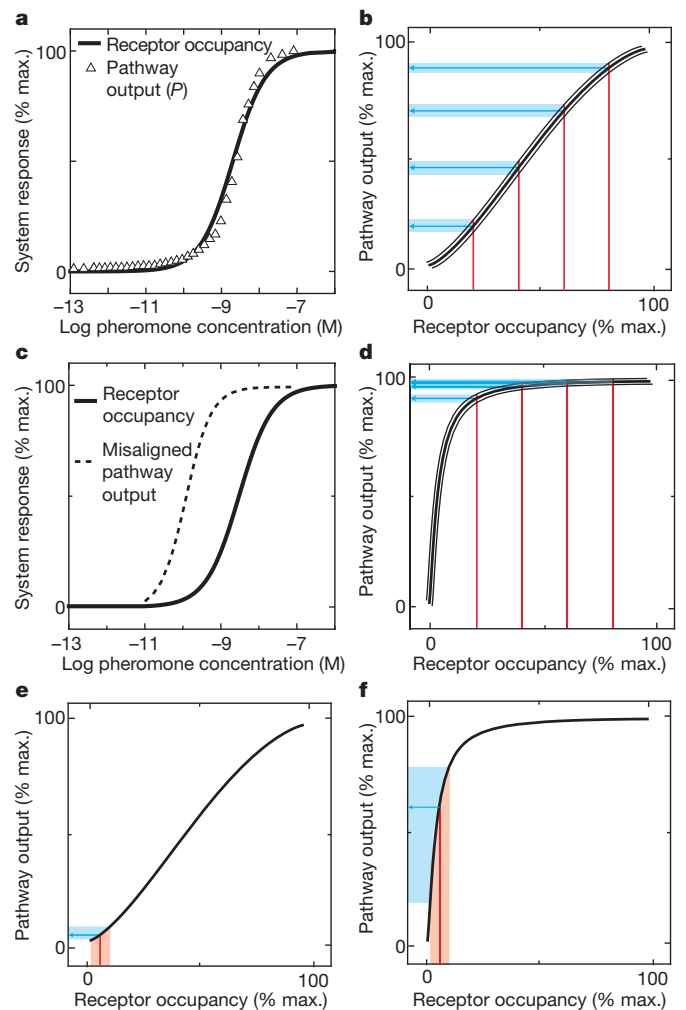


Figure 2 | Dose-response alignment makes responses more distinguishable. **a**, Dose responses of receptor occupancy (calculated from reported receptor–pheromone binding affinity measurements^{45,46}) and reporter gene expression output corrected for known sources of cell-to-cell variation (pathway output P^5) align closely. **b**, The relationship between receptor occupancy and downstream response (from **a**) is essentially linear. Evenly distributed receptor occupancies (20%, 40%, 60% and 80%, red vertical lines) correspond to evenly spaced downstream responses (blue horizontal lines). **c**, Example of dose-response misalignment, in which the downstream output is 20-fold more sensitive than that in **a** (that is, the EC_{50} is reduced 20-fold). **d**, Dose-response misalignment makes transfer function nonlinear, which compresses the downstream responses (blue horizontal lines) corresponding to the majority of receptor occupancies (red vertical lines), making downstream responses less distinguishable. **e, f**, Dose-response misalignment results in noise amplification. Receptor occupancy (red vertical line) with noise (pink spread) yields downstream responses (horizontal blue lines) with associated noise (blue spread). In the system with dose-response alignment (**e**), linear transfer function yields less relative noise in the downstream response than in the system with misaligned dose responses and nonlinear transfer function (**f**).

alignment minimizes the amplification of upstream noise (Fig. 2e). Previous analysis of noise propagation in a synthetic gene circuit revealed analogous amplification of upstream noise in a system with misaligned dose responses¹⁶. This reasoning suggested to us that cell signalling systems with misaligned dose responses inherently transmit information with lower fidelity, even if downstream responses are not saturated, an idea consistent with previous observations that hypersensitive cells oriented mating projections less precisely in gradients than wild-type cells even at concentrations that did not saturate downstream responses³. We hypothesized that dose-response alignment might be indicative of a system that can transmit large

amounts of information, and therefore we sought to understand better the underlying molecular mechanisms required for dose–response alignment and the linear relationship between upstream and downstream response that it defines.

Work in electronics in the 1930s established that ‘proportional’ negative feedback in electrical circuits, where a constant fraction of the output is subtracted from the input, can bring about a linear input–output voltage relationship¹⁷. Biologists have also shown that negative feedback can make input–output relationships more linear in biological systems: for example, it was shown that in a MAPK/protein kinase C (PKC)-mediated signalling system, increasing the amount of a MAPK-activated phosphatase that inactivates the MAPK made the average output response more linearly related to (that is, proportional to) the input¹⁸. Research in both biology and engineering^{17,19–22} has also suggested or shown that negative feedback can increase the signal-to-noise ratio in system output and decrease the sensitivity of output to variation in properties of system components (see Supplementary Information 8 for further discussion). These observations suggested to us that negative feedback might mediate dose–response alignment and improve information transmission in the yeast pheromone response system.

Previous work showed that the pheromone response system quickly establishes dose–response alignment: the accumulation of reporter gene expression in cells increased linearly from 15 min to 3 h after stimulation (see Fig. 2 in ref. 5), and at all times the normalized dose response of downstream output aligned with the receptor–ligand-binding curve. These facts suggested that the molecular mechanisms that bring about and stabilize dose–response alignment occur in the first 15 min of pheromone stimulation. However, no quantitative measurements of system activities in this time frame existed to indicate the action of negative feedback to align dose responses. We therefore developed tools to measure the early dynamics of molecular events that the system uses to operate before, during and after establishment of dose–response alignment.

Initial system dynamics indicate negative feedback

We developed reporters and methods to measure real-time signal transmission in single cells, at the membrane and in the nucleus, and supplemented these data with biochemical measurements. We then measured system outputs (that is, system activities at different stages in the signalling pathway, see Fig. 1) after stimulating cells with 100 nM pheromone, a concentration that produces maximal downstream transcription reporter response (Fig. 2a).

Two membrane-proximal system outputs, G-protein activation and Ste5 recruitment to the membrane, peaked and declined rapidly. To follow G-protein activation in single cells over time, we measured loss of fluorescence resonance energy transfer (FRET) between cyan fluorescent protein (CFP)-tagged Gpa1 and yellow fluorescent protein (YFP)-tagged Ste18 by image cytometry²³ (Supplementary Information 2) in a derivative of a strain developed previously⁶. Loss of G-protein FRET rapidly peaked in the first minute and declined (Fig. 3a and Supplementary Fig. 2), consistent with lower time resolution, single-time-point population measurements in an earlier study⁶.

We then measured, also in single cells and at subminute intervals, a subsequent membrane-proximal signalling event, the recruitment of Ste5 to the membrane. To do this, we measured the redistribution of YFP–Ste5 from the nucleus and cytosol to the membrane (Supplementary Information 2). Membrane recruitment of Ste5 was rapid (Fig. 3b). Within 5 s of stimulation with a high concentration of pheromone, individual cells showed an increase in yellow fluorescence at the cell membrane, and a corresponding depletion of fluorescence from the cell interior—no change in fluorescence was observed in unstimulated cells or cells with unlabelled Ste5 (Supplementary Fig. 3). Compared with unstimulated cells, average membrane recruitment reached near-maximal values within seconds and peaked by 20 s, before declining towards a plateau in later minutes, similar to the dynamics of G-protein loss of FRET.

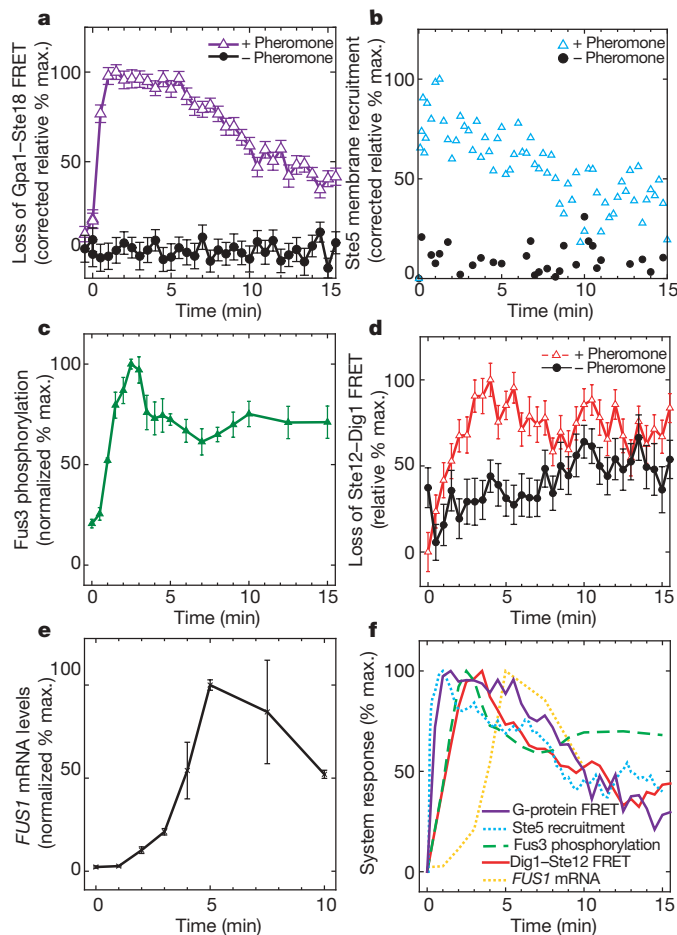


Figure 3 | Initial system dynamics indicate negative feedback. **a**, Loss of G-protein FRET. Corrected median (\pm standard error) loss of Gpa1–Ste18 FRET values (relative to maximum change measured in pheromone-stimulated cells; see Supplementary Fig. 2) in RY2062b cells stimulated with pheromone (purple triangles; $n = 262$) quickly peaked and declined to a plateau relative to unstimulated cells (black circles; $n = 143$). **b**, YFP–Ste5 recruitment. Corrected median (\pm standard error) YFP–Ste5 membrane recruitment (relative to maximum change measured in pheromone-stimulated cells; see Supplementary Fig. 3e) in RY2013 cells stimulated with pheromone stimulation (cyan triangles, $n = 361$) quickly peaked and declined to a plateau compared to unstimulated cells (black circles, $n = 223$). **c**, Fus3 activity. Mean ratios (\pm standard error, $n = 3–5$) of activated (phospho-Y180 and phospho-T182) Fus3 to total Fus3, normalized to the peak measured ratio (see Supplementary Fig. 4 for representative immunoblot images). Fus3 activity levels peaked 2.5 min after pheromone stimulation and declined to a plateau within 5 min of stimulation. Total Fus3 levels, compared to levels of non-pheromone-regulated proteins GAPDH and PGK1, remained constant over this time period (data not shown). New protein synthesis is not required for the observed peak and decline (Supplementary Fig. 4c). **d**, Loss of Dig1–Ste12 FRET. Median (\pm standard error) loss of Dig1–Ste12 FRET (scaled to minimum and maximum values measured in pheromone-stimulated cells; for raw values, see Supplementary Fig. 7) in RY1130b cells peaked about 3 min after pheromone stimulation, and then declined to a plateau relative to unstimulated cells (black circles, $n = 138$). **e**, *FUS1* mRNA. Average ratio (high and low values indicated) of *FUS1* mRNA probe band intensity to loading control (*ACT1* mRNA probe band intensity) after pheromone stimulation ($n = 2$) (see Supplementary Fig. 8 for raw image). **f**, Composite timing plot shows persistent peak-and-decline towards a plateau for all system responses, suggesting action of negative feedback. YFP–Ste5 recruitment and Dig1–Ste12 FRET (from **b** and **d**) were smoothed using a moving window of five data points.

We then assessed intermediate system output farther downstream by measuring the dynamics of MAPK activation. Using quantitative immunoblotting, we measured phosphorylation of Fus3 residues

Thr 180 and Tyr 182, which is required for Fus3 activity and pheromone response²⁴. The amount of phosphorylated Fus3 relative to total Fus3 increased rapidly, reaching a maximum in 2.5 min before dropping to a plateau level in approximately 5–7 min (Fig. 3c and Supplementary Fig. 4a, b).

We then measured nuclear MAPK activity dynamics in single cells over time. To do this we developed a FRET reporter to measure pheromone-induced changes in the association between the transcription factor Ste12 and one of its inhibitors, Dig1 (ref. 25). We deleted native *STE12* and *DIG1* genes and chromosomally integrated versions of these proteins fused to CFP and YFP, respectively (see Supplementary Information 5). We then measured changes in FRET between CFP and YFP²⁶ in the nucleus by image cytometry²³ (see Supplementary Fig. 6 and Supplementary Information 2). Pheromone-induced loss of FRET did not require new protein translation (Supplementary Fig. 7b), but did require both Ste5 (Fig. S7c) and MAPK activity (Supplementary Fig. 7d), consistent with the interpretation that loss of FRET directly reports pheromone-induced, MAPK-mediated de-repression of Ste12.

Loss of Dig1–Ste12 FRET quickly peaked around 3 min after stimulation (Fig. 3d), and the overall signal dynamics were very similar to those of Fus3 phosphorylation (compare Fig. 3c to Fig. 3d; see also Fig. 3f). This fast signal transfer from Fus3 activation to Ste12 de-repression is consistent with the idea that Fus3 moves quickly in and out of the nucleus, as shown in studies of changes in Fus3 localization by fluorescence recovery after photobleaching (FRAP)²⁷. We confirmed that the timing of Ste12 de-repression measured by loss of Ste12–Dig1 FRET was consistent with the dynamics of pheromone-induced mRNA transcription. Using RNase protection assays, we quantified *FUS1* mRNA levels. *FUS1* mRNA levels peaked at 5 min after pheromone stimulation before declining

(Fig. 3e and Supplementary Fig. 8). The maximum rate of increase in mRNA occurred between 3 and 5 min, consistent with the time of maximum loss of Ste12–Dig1 FRET.

All measurements of signal-relaying events showed a consistent pattern of rapid peak and decline towards a plateau after pheromone stimulation (Fig. 3f), which suggested the action of one or more fast-acting negative feedbacks that might modulate the dose-dependence of the signal to achieve dose–response alignment.

Fus3 mediates negative feedback

A number of previous studies suggested that the MAPKs Fus3 and Kss1 might mediate rapid negative feedback. Our previous study of regulated cell-to-cell variation in system output revealed a Fus3-dependent reduction in variation, suggesting an autoregulatory negative feedback mediated by Fus3 (ref. 5). One study showed that levels of phosphorylated Fus3 were higher in cells bearing a kinase-dead mutant version of Fus3 (ref. 24). Another study showed that Ste5(T287A) mutant cells, in which the Ste5 protein is mutated at the site of a threonine residue phosphorylated by Fus3 on Ste5-derived peptides *in vitro*, showed increased reporter expression²⁸, albeit with no change in the EC₅₀ of the dose response. Another study found that glutamate substitutions at candidate sites of Fus3 phosphorylation on Ste7 decreased on-scaffold Fus3 activation and mating efficiency²⁹. Additionally, phosphoproteomic studies of pheromone response system proteins³⁰ have uncovered numerous sites of phosphorylation on system proteins, and many of these phosphor-

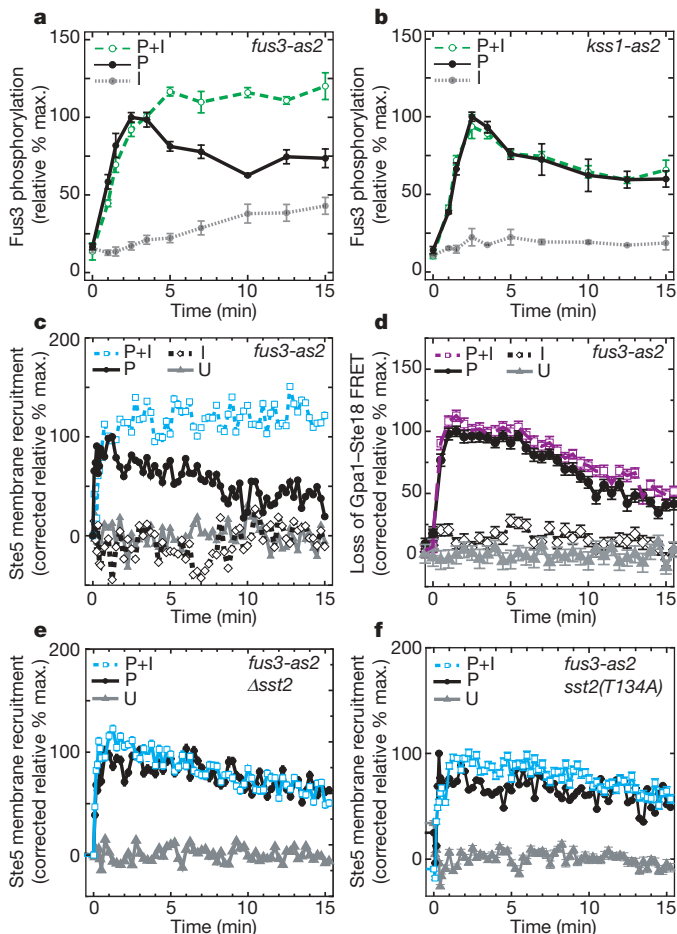


Figure 4 | Fus3 mediates negative feedback. Values are scaled to peak signal measured in cells stimulated with only pheromone. Error bars indicate \pm standard error for all panels: P, stimulated with 100 nM pheromone; P+I, stimulated with 100 nM pheromone plus 10 μ M 1-NM-PP1; I, 10 μ M 1-NM-PP1; U, untreated. **a**, Fus3 mediates negative feedback. In *fus3-as2* cells (RY1134b), mean ($n = 4$) Fus3 phosphorylation peaked and declined, as in *FUS3* cells (Fig. 3b), after pheromone stimulation (black circles), but did not decline when we stimulated cells simultaneously with Fus3-as2 inhibitor (green circles). Treating cells with only inhibitor (grey circles) caused the signal to rise slowly, indicating that cells actively regulate basal signal level. **b**, Kss1 does not mediate negative feedback. In *kss1-as2* cells (RY1133b), mean ($n = 4$) Fus3 phosphorylation in pheromone-stimulated cells without (black circles) or with (green circles) simultaneous treatment with Kss1-as2 inhibitor were identical. Treating cells with only inhibitor caused no significant increase in Fus3 phosphorylation (grey circles). **c**, Fus3-mediated feedback acts on or upstream of Ste5 membrane recruitment. In *fus3-as2* cells (RY2013), median YFP–Ste5 membrane recruitment peaked and declined after pheromone stimulation (filled circles; $n = 361$), but did not decline after simultaneous treatment with Fus3-as2 inhibitor (blue squares; $n = 196$). There was no relative Ste5 recruitment in cells treated with inhibitor alone (open diamonds; $n = 134$) or in completely untreated cells (grey triangles; $n = 220$). The small increase in Fus3 phosphorylation measured in cells treated with inhibitor only (black circles in **a**) suggests that additional Fus3-independent mechanisms maintain low basal levels of Ste5 recruitment. **d**, Fus3-mediated negative feedback acts downstream of G-protein dissociation. In *fus3-as2* cells (RY2062b, derived from TMY101 (ref. 6)), median Gpa1–Ste18 loss of FRET peaked and declined in pheromone-stimulated cells (filled circles; $n = 262$) with the same dynamics as in pheromone-stimulated cells simultaneously treated with Fus3-as2 inhibitor (purple squares; $n = 263$). Unstimulated cells in the presence (open diamonds; $n = 229$) or absence (grey triangles; $n = 143$) of inhibitor showed no loss of Gpa1–Ste18 FRET. **e**, One target of Fus3-mediated negative feedback is a novel Sst2-dependent increase in YFP–Ste5 recruitment. Median YFP–Ste5 membrane recruitment in pheromone-stimulated *fus3-as2 Δsst2* cells (RY2024) peaked and declined both in the absence (black circles; $n = 188$) or presence (cyan squares; $n = 300$) of Fus3-as2 inhibitor, similar to *SST2* cells with active Fus3 (black circles, panel **c**). Grey triangles indicate unstimulated cells ($n = 268$). **f**, Mutation of predicted Fus3/MAPK phosphorylation site in Sst2 DEP1 domain eliminated Sst2 promotion of YFP–Ste5 recruitment. Median (\pm standard error) YFP–Ste5 membrane recruitment in pheromone-stimulated *sst2(T134A)* (RY2077) cells peaked and declined both in the absence (filled circles; $n = 309$) and presence (cyan squares; $n = 321$) of inhibitor, similar to *Δsst2* cells (panel **e**). Grey triangles indicate unstimulated cells ($n = 334$).

ylation sites lie in consensus MAPK target sequences (R. Maxwell and O. Resnekov, personal communication). Finally, work with one pheromone response system model showed that feedbacks, including one from Fus3, increased the alignment of upstream and downstream dose responses³¹. We therefore proposed that the signal decline at different measurement points depends on non-translational, fast-acting negative feedbacks mediated by Fus3 or Kss1.

To test whether Fus3 or Kss1 is a source of negative feedback on system activity, we compared the baseline system response, at system points up to and including Fus3 phosphorylation, with system response after selective inhibition of either Fus3 or Kss1 kinase activity. To do this, we first modified reporter strains by replacing either *FUS3* or *KSS1* with the corresponding purine-analogue-sensitive allele³². We did this by changing the 'gatekeeper' residue in each kinase's ATP binding pocket (Q93 in Fus3; N94 in Kss1) to an alanine. The mutant *fus3-as2* and *kss1-as2* kinases were active, as measured by fluorescent protein reporter gene output (Supplementary Fig. 9a), and 10 μ M 4-amino-1-(tert-butyl)-3-(1'-naphthylmethyl)-pyrazolo[3,4-*d*]pyrimidine (1-NM-PP1), a cell-permeable adenosine analogue, inhibited the activity of mutant kinases without inhibiting wild-type kinases (Supplementary Fig. 9b). We then quantified Fus3 phosphorylation by quantitative immunoblotting after stimulation with pheromone, either with or without simultaneous inhibition with 1-NM-PP1 (Fig. 4a). Fus3 phosphorylation levels did not peak and decline to a plateau when we inhibited Fus3-*as2*, but, rather, remained high, near peak levels. By contrast, when we inhibited Kss1-*as2*, Fus3 phosphorylation levels were unaffected (Fig. 4b). These results indicated that Fus3 kinase activity mediated one or more negative feedbacks in this system.

We then studied where in the system the Fus3-dependent feedback acted to diminish signal amplitude. The decrease in G-protein FRET within 30 s of stimulation depends on Sst2 (ref. 6). This finding suggested that the Fus3-dependent negative feedback might upregulate the GTPase-activating protein (GAP) function of Sst2, which would increase G-protein re-association and decrease downstream signal. We tested whether Fus3-*as2* inhibition affected the observed decline in both G-protein dissociation and Ste5 recruitment. Inhibition of Fus3 activity eliminated the decline in Ste5 translocation (Fig. 4c), but surprisingly had no effect on the decline in G-protein dissociation in a G-protein FRET reporter strain carrying *fus3-as2* (Fig. 4d and Supplementary Fig. 10). These results indicated that Fus3-mediated negative feedback acted downstream of mechanisms regulating G-protein association.

To confirm that Fus3 acted downstream of G-protein activation, we measured Ste5 recruitment after deleting *SST2*. We expected deletion of *SST2* to have no effect on Fus3-mediated signal decline, as Sst2 is required for efficient G-protein inactivation and, as we showed above, Fus3-mediated negative feedback does not reduce G-protein dissociation levels. Unexpectedly, when we deleted *SST2*, we completely disrupted Fus3-mediated signal decline; unlike *SST2*⁺ cells, inhibition of Fus3 did not cause an increase in Ste5 recruitment (Fig. 4e). Furthermore, Ste5 recruitment (with or without Fus3-mediated feedback) peaked and declined similar to the baseline response of *SST2*⁺ cells (compare squares and circles in Fig. 4e with circles in Fig. 4c). This finding showed that signal peak and decline is the default behaviour in the absence of Sst2. Because a sustained non-declining signal is only evident in *SST2*⁺ cells in the presence of Fus3-*as2* inhibitor, these results also indicate that Sst2 promotes the Ste5 membrane recruitment, a hitherto unknown function of the regulator of G-protein signalling (RGS) protein family, and that Fus3 negatively regulates this novel signal-promoting function (Fig. 5a).

We then investigated which portions of the Sst2 protein might be involved in promoting Ste5 membrane recruitment. During analysis of Sst2 point mutants, we found that Ste5 recruitment in a *fus3-as2* strain that carried *sst2(T134A)* instead of wild-type Sst2 peaked and declined in the presence and absence of Fus3 inhibitor (Fig. 4f), just as observed in Δ *Sst2* cells (Fig. 4e). The pheromone-induced growth

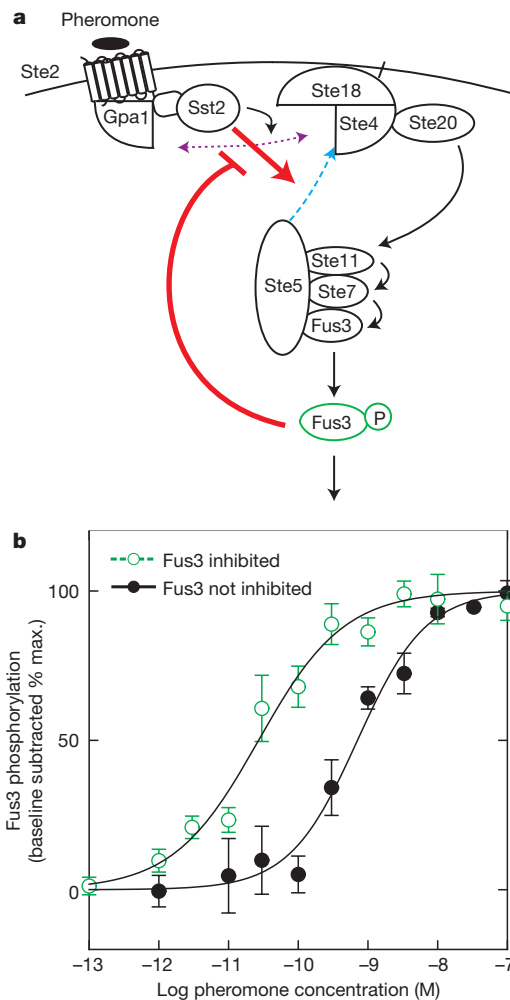


Figure 5 | Dose-response alignment requires Fus3-mediated negative feedback. **a**, Model of negative feedback regulation of Ste5 membrane recruitment. Sst2 promotes (thick red arrow) Ste5 recruitment to the membrane (blue dashed arrow), and Fus3 negatively regulates this signal promoting (thick T-bar arrow). **b**, Fus3 inhibition disrupts dose-response alignment. In pheromone-stimulated *fus3-as2* (RY2052b) cells, inhibition of Fus3 kinase activity (green circles) reduced the sensitivity (EC_{50}) of the dose response of mean Fus3 phosphorylation (\pm standard error; $n = 3-4$) relative to cells not treated with inhibitor (black filled circles). This measured dose response of Fus3 phosphorylation in uninhibited cells is approximately ten times more sensitive than a previous measurement in a different strain background⁴⁷. Fus3 phosphorylation was measured after 15 min of pheromone stimulation, after the signal reaches the dose-dependent plateau (see Fig. 3c). Black lines show fits to Hill functions. Fus3 inhibition reduced the EC_{50} of the dose response by greater than 20-fold without affecting the gradedness (cooperativity) of the average response (see Supplementary Information for details).

inhibition of *sst2(T134A)* cells reported by halo assays was close to wild-type levels (Supplementary Fig. 11a), and the average number of Sst2(T134A) protein molecules per cell was similar to Sst2 abundance in the parent strain (Supplementary Fig. 11b), suggesting that the T134A mutation disrupts a significant fraction of the Fus3-dependent, signal-promoting function of Sst2 without disrupting the bulk of its signal-reducing GAP activity. T134 lies within the N-terminal DEP domains of Sst2, which are required for localization of Sst2 to the membrane by binding the cytosolic tail of Ste2 (ref. 33). These results indicate that the DEP domains in Sst2 might aid Ste5 membrane recruitment, perhaps by providing additional membrane-proximal interaction surfaces, and suggest that mechanisms that regulate localization of Sst2 to the membrane, such as disruption of Sst2-Ste2 interactions by Yck1/2-mediated phosphorylation after

longer periods of pheromone stimulation³³, might consequently regulate Ste5 membrane recruitment.

Fus3-generated negative feedback aligns dose responses

Finally, we tested whether dose–response alignment between receptor–pheromone binding and downstream activities required Fus3 activity. In principle, Fus3-mediated negative feedback might scale system activity by a dose-independent factor, and therefore cause no shift in the normalized dose–response curve. For example, the Ste5(T287A) mutation increases the magnitude of system output relative to wild-type cells without changing the pheromone concentration yielding half-maximal response (see Fig. 5 in ref. 28). We measured dose responses of Fus3 phosphorylation in a *fus3-as2* strain with and without inhibitor 15 min after pheromone stimulation, the time when the amount of Fus3 phosphorylation had declined to a steady-state level (Fig. 3c). Inhibiting Fus3 kinase activity shifted the dose response of Fus3 activation, lowering the pheromone concentration needed for half-maximal response by 20-fold (Fig. 5b). Moreover, Fus3-mediated negative feedback reduces the dynamic range of the output by only 50% (see Supplementary Information 8.2 and Supplementary Fig. 14). These results showed that Fus3-mediated negative feedback was required for dose–response alignment in the yeast pheromone response system.

Discussion

We found that MAPK Fus3 mediates rapid negative feedback that aligns the dose responses of upstream and downstream system activities in the pheromone response system. We propose that dose–response alignment improves information transmission through this and other signalling systems. Furthermore, we found that Fus3 negatively regulates a novel signal-promoting function of the RGS protein Sst2. Our results demonstrate that RGS proteins, present in many eukaryotic signalling systems (the human RGS family, for example, contains more than 35 members³⁴), can function in signal transduction systems by increasing signal in addition to accelerating G-protein inactivation, possibly (as in the case of pheromone response) by facilitating recruitment of MAPK scaffolds to sites of activity.

The idea that dose–response alignment increases the amount of transmitted information has practical implications for drug discovery and design. For example, consider a drug that increased the sensitivity of cells to a naturally occurring antagonist of cell proliferation, analogous to the downstream dose–response shift we observed on Fus3 inhibition in the pheromone response system (Fig. 5b). Despite increasing the average sensitivity of cells to signals to stop growth, the dose–response misalignment could reduce the amount of transmitted information about the signal. The decrease in transmitted information could increase cell-to-cell variation in response, causing a larger number of cells to fall below a threshold in antagonist response and continue proliferation. It is possible that some existing drugs that allosterically modify G-protein-coupled receptor signalling systems downstream of ligand binding (see Fig. 3 in ref. 35) and those that target mid-system signalling molecules such as PKC³⁶ and AKT³⁷ may decrease dose–response alignment and increase response variation, whereas drugs that specifically affect the affinity of receptor–ligand binding (see Fig. 5 in ref. 35) should not.

We propose here that the fidelity with which a cell responds to different input concentrations of a ligand depends on a ‘systems-level’ quantitative behaviour, dose–response alignment, found in many other cell signalling systems. For biological systems, a deeper understanding of key quantitative behaviours will probably depend on articulating appropriate analytical frameworks and metrics. Information theory³⁸ defines a framework for quantifying the relationship between system input and output (see Supplementary Information 9 for further discussion), and has enabled researchers to quantify, for example, the amount of information that an axon of a single sensory neuron can transmit³⁹ and the amount of information

about morphogen gradient that a transcription factor can transmit to a downstream effector^{40,41}. In much the same way as concepts from classical electromagnetism provide rigorous means to describe and understand the determinants of behaviours of electrical circuits, we expect that concepts from information theory will enable more rigorous and quantitative understanding of how the protein components of complex vertebrate cell signalling systems interact to sense and transmit information into the cell.

METHODS SUMMARY

We constructed yeast strains and plasmids by standard methods^{42,43} essentially as described (ref. 5 and Supplementary Information 1). By doctrine, we expressed all reporter constructs from native promoters integrated into the chromosome, and verified that the level of expressed protein was similar to the native level. With the exception of strains used for G-protein FRET experiments, we constructed all strains from the otherwise-isogenic *bar1⁻ W303a* reference parent strain, ACL 379 (ref. 5), by the steps described. We stimulated exponentially growing cells with the indicated concentration of pheromone and/or other reagents (such as the inhibitor 1-NM-PP1) in one of two ways. For image cytometry, we affixed the cells to the bottom of wells in a glass-bottom 96-well plate, as described previously⁵ and in Supplementary Information 2.1. Using custom fluidic hardware, we evacuated medium from the well, injected fresh medium containing the indicated concentration of pheromone and/or inhibitor, and proceeded to record images over time. For MAPK phosphorylation, *FUS1* mRNA, and flow cytometry experiments, we stimulated cells by using a micropipette to mix a small volume of pheromone and/or inhibitor into the cell suspension to the final concentration (as indicated, typically 100 nM pheromone and 10 μ M 1-NM-PP1). We performed image acquisition essentially as described^{5,23}, with modifications as detailed in Supplementary Information. For image cytometry, we extracted values for parameters of interest from images using Cell-ID 1.0 (ref. 23). We analysed image and flow cytometric data using Physics Analysis Workstation (see ref. 44) and custom scripts, depending on the type of image, described in the text and in Supplementary Information. Supplementary Information contains further details on plasmids, strains, construction methods, materials and experimental methods.

Received 23 December 2007; accepted 3 October 2008.

- Dohlman, H. G. & Thorner, J. W. Regulation of G protein-initiated signal transduction in yeast: Paradigms and principles. *Annu. Rev. Biochem.* **70**, 703–754 (2001).
- Jackson, C. L. & Hartwell, L. H. Courtship in *S. cerevisiae*: Both cell types choose mating partners by responding to the strongest pheromone signal. *Cell* **63**, 1039–1051 (1990).
- Segall, J. E. Polarization of yeast cells in spatial gradients of alpha mating factor. *Proc. Natl Acad. Sci. USA* **90**, 8332–8336 (1993).
- Schrick, K., Garvik, B. & Hartwell, L. H. Mating in *Saccharomyces cerevisiae*: The role of the pheromone signal transduction pathway in the chemotropic response to pheromone. *Genetics* **147**, 19–32 (1997).
- Colman-Lerner, A. et al. Regulated cell-to-cell variation in a cell-fate decision system. *Nature* **437**, 699–706 (2005).
- Yi, T. M., Kitano, H. & Simon, M. I. A quantitative characterization of the yeast heterotrimeric G protein cycle. *Proc. Natl Acad. Sci. USA* **100**, 10764–10769 (2003).
- Cuatrecasas, P. Insulin–receptor interactions in adipose tissue cells: Direct measurement and properties. *Proc. Natl Acad. Sci. USA* **68**, 1264–1268 (1971).
- Kasai, M. & Changeux, J. P. *In vitro* excitation of purified membrane by cholinergic agonists. *J. Membr. Biol.* **6**, 58–80 (1971).
- Amir, S. M., Carraway, T. F. Jr, Kohn, L. D. & Winand, R. J. The binding of thyrotropin to isolated bovine thyroid plasma membranes. *J. Biol. Chem.* **248**, 4092–4100 (1973).
- Lin, S. Y. & Goodfriend, T. L. Angiotensin receptors. *Am. J. Physiol.* **218**, 1319–1328 (1970).
- Knauer, D. J., Wiley, H. S. & Cunningham, D. D. Relationship between epidermal growth factor receptor occupancy and mitogenic response. Quantitative analysis using a steady state model system. *J. Biol. Chem.* **259**, 5623–5631 (1984).
- Nagashima, T. et al. Quantitative transcriptional control of ErbB receptor signaling undergoes graded to biphasic response for cell differentiation. *J. Biol. Chem.* **282**, 4045–4056 (2007).
- Simons, S. S. Jr, Oshima, H. & Szapary, D. Higher levels of control: Modulation of steroid hormone-regulated gene transcription. *Mol. Endocrinol.* **6**, 995–1002 (1992).
- Rousseau, G. G. & Baxter, J. D. Glucocorticoid receptors. *Monogr. Endocrinol.* **12**, 49–77 (1979).
- Bloom, E. et al. Nuclear binding of glucocorticoid receptors: Relations between cytosol binding, activation and the biological response. *J. Steroid Biochem.* **12**, 175–184 (1980).

16. Pedraza, J. M. & van Oudenaarden, A. Noise propagation in gene networks. *Science* **307**, 1965–1969 (2005).
17. Black, H. S. Stabilized feed-back amplifiers. *Electr. Eng.* **53**, 114–120 (1934).
18. Bhalla, U. S., Ram, P. T. & Iyengar, R. MAP kinase phosphatase as a locus of flexibility in a mitogen-activated protein kinase signaling network. *Science* **297**, 1018–1023 (2002).
19. Black, J. W. & Lefkowitz, P. Operational models of pharmacological agonism. *Proc. R. Soc. Lond. B* **220**, 141–162 (1983).
20. Savageau, M. A. Comparison of classical and autogenous systems of regulation in inducible operons. *Nature* **252**, 546–549 (1974).
21. Becskei, A. & Serrano, L. Engineering stability in gene networks by autoregulation. *Nature* **405**, 590–593 (2000).
22. Barkai, N. & Leibler, S. Robustness in simple biochemical networks. *Nature* **387**, 913–917 (1997).
23. Gordon, A. *et al.* Single-cell quantification of molecules and rates using open-source microscope-based cytometry. *Nature Methods* **4**, 175–181 (2007).
24. Gartner, A., Nasmyth, K. & Ammerer, G. Signal transduction in *Saccharomyces cerevisiae* requires tyrosine and threonine phosphorylation of Fus3 and Kss1. *Genes Dev.* **6**, 1280–1292 (1992).
25. Tedford, K., Kim, S., Sa, D., Stevens, K. & Tyers, M. Regulation of the mating pheromone and invasive growth responses in yeast by two map kinase substrates. *Curr. Biol.* **7**, 228–238 (1997).
26. Miyawaki, A. & Tsien, R. Y. Monitoring protein conformations and interactions by fluorescence resonance energy transfer between mutants of green fluorescent protein. *Methods Enzymol.* **327**, 472–500 (2000).
27. van Drogen, F., Stucke, V. M., Jorritsma, G. & Peter, M. Map kinase dynamics in response to pheromones in budding yeast. *Nature Cell Biol.* **3**, 1051–1059 (2001).
28. Bhattacharyya, R. P. *et al.* The ste5 scaffold allosterically modulates signaling output of the yeast mating pathway. *Science* **311**, 822–826 (2006).
29. Maleri, S. *et al.* Persistent activation by constitutive Ste7 promotes Kss1-mediated invasive growth but fails to support Fus3-dependent mating in yeast. *Mol. Cell Biol.* **24**, 9221–9238 (2004).
30. Gruhler, A. *et al.* Quantitative phosphoproteomics applied to the yeast pheromone signaling pathway. *Mol. Cell Proteomics* **4**, 310–327 (2005).
31. Shao, D., Zheng, W., Qiu, W., Ouyang, Q. & Tang, C. Dynamic studies of scaffold-dependent mating pathway in yeast. *Biophys. J.* **91**, 3986–4001 (2006).
32. Bishop, A. C. *et al.* A chemical switch for inhibitor-sensitive alleles of any protein kinase. *Nature* **407**, 395–401 (2000).
33. Ballon, D. R. *et al.* DEP-domain-mediated regulation of GPCR signaling responses. *Cell* **126**, 1079–1093 (2006).
34. Heximer, S. P. & Blumer, K. J. RGS proteins: Swiss army knives in seven-transmembrane domain receptor signaling networks. *Sci. STKE* **2007**, pe2 (2007).
35. May, L. T., Leach, K., Sexton, P. M. & Christopoulos, A. Allosteric modulation of G protein-coupled receptors. *Annu. Rev. Pharmacol. Toxicol.* **47**, 1–51 (2007).
36. Budas, G. R., Churchill, E. N. & Mochly-Rosen, D. Cardioprotective mechanisms of PKC isozyme-selective activators and inhibitors in the treatment of ischemia-reperfusion injury. *Pharmacol. Res.* **55**, 523–536 (2007).
37. Lindsley, C. W., Barnett, S. F., Layton, M. E. & Bilodeau, M. T. The PI3K/Akt pathway: Recent progress in the development of ATP-competitive and allosteric Akt kinase inhibitors. *Curr. Cancer Drug Targets* **8**, 7–18 (2008).
38. Shannon, C. A mathematical theory of communication. *Bell Syst. Tech. J.* **27**, 379–423 (1948).
39. Bialek, W., Rieke, F., de Ruyter van Steveninck, R. R. & Warland, D. Reading a neural code. *Science* **252**, 1854–1857 (1991).
40. Tkacik, G., Callan, C. & Bialek, W. Information flow and optimization in transcriptional regulation. *Proc. Natl. Acad. Sci. U.S.A.* **26**, 12265–12270 (2008).
41. Gregor, T., Tank, D. W., Wieschaus, E. F. & Bialek, W. Probing the limits to positional information. *Cell* **130**, 153–164 (2007).
42. Ausubel, F. M. *et al.* *Current Protocols in Molecular Biology* (John Wiley & Sons, Inc., 1987–2008).
43. Guthrie, C. & Fink, G. R. *Methods in Enzymology, Guide to Yeast Genetics and Molecular Biology* (Academic, 1991).
44. Brun, R., Couet, O., Vandroni, C. & Zanarini, O. PAW Physics Analysis Workstation CERN program library entry q121 (CERN, Geneva, 1989).
45. Jenness, D. D., Burkholder, A. C. & Hartwell, L. H. Binding of alpha-factor pheromone to *Saccharomyces cerevisiae* cells: Dissociation constant and number of binding sites. *Mol. Cell Biol.* **6**, 318–320 (1986).
46. Bajaj, A. *et al.* A fluorescent α -factor analogue exhibits multiple steps on binding to its g protein coupled receptor in yeast. *Biochemistry* **43**, 13564–13578 (2004).
47. Andersson, J., Simpson, D. M., Qi, M., Wang, Y. & Elion, E. A. Differential input by Ste5 scaffold and Msg5 phosphatase route a MAPK cascade to multiple outcomes. *EMBO J.* **23**, 2564–2576 (2004).

Supplementary Information is linked to the online version of the paper at www.nature.com/nature.

Acknowledgements We thank P. Abola, S. Andrews, A. Arkin, M. Bowen, L. Buck, C. Denby, A. Gann, D. Meldrum, T. Mitchison, C. Pabo, M. Ptashne, M. Reese, O. Resnekov, C. Ryan, M. Snyder, T. Thomson, A. E. Tsong and M. Wilson for discussions and/or comments on the manuscript, and O. Resnekov for help in articulating the requirements for fluidic induction devices. Work, including that of M.H. at the University of Washington, was supported by the Alpha Project at the Center for Quantitative Genome Function, an NIH Center of Excellence in Genomic Science under grant P50 HG02370 from the National Human Genome Research Institute to R.B.

Author Contributions R.C.Y. performed the Ste5 translocation, loss of G-protein and Dig1–Ste12 FRET, MAP kinase phosphorylation, mRNA measurements, and the image-based measurements of system output. C.G.P. and A.G. noted and helped articulate the relationship of negative feedback to dose–response overlap. C.G.P. and R.C.Y. performed flow cytometric measurements. L.L. and A.G. contributed to discussions about mutual information calculations and analysis. R.C.Y. and A.G. performed data analysis on loss of FRET experiments. A.C.-L. and A.G. carried out extensive initial measurements of Ste5 recruitment. K.B. provided unpublished information about protein quantification useful in initial discussions about dose–response alignment. R.C.Y. and D.P. performed numerous measurements verifying protein abundance in other strains. E.S. constructed the inhibitor-sensitive *fus3-as2* and *kss1-as2* alleles. M.H. designed and built fluidic devices used to induce the system in response to articulated requirements. R.B. provided input into project direction, experimental design and interpretation of results. R.C.Y., C.G.P. and R.B. wrote the paper and guarantee the integrity of the results.

Author Information Reprints and permissions information is available at www.nature.com/reprints. Correspondence and requests for materials should be addressed to ryu@molsci.org and brent@molsci.org.